^{18}O ^{48}Ti elastic and inelastic scattering at 275 MeV

G. A. Brischetto,[1,2,*] O. Sgouros,[1,2] D. Carbone,[2] F. Cappuzzello,[1,2] M. Cavallaro,[2] J. Lubian,[3] G. De Gregorio,[4,5] C. Agodi,[2] D. Calvo,[6] E. R. Chávez Lomelí,[7] I. Ciraldo,[1,2] F. Delaunay,[1,2,8] H. Djapo,[9] C. Eke,[10] P. Finocchiaro,[2] M. Fisichella,[2] A. Gargano,[4] M. A. Guazzelli,[11] A. Hacisalihoglu,[12] R. Linares,[3] N. H. Medina,[13] M. Moralles,[13] J. R. B. Oliveira,[14] A. Pakou,[15] L. Pandola,[2] V. Soukeras,[1,2] G. Souliotis,[16] A. Spatafora,[2] D. Torresi,[2] A. Yildirim,[17] and V. A. B. Zagatto[14]

(NUMEN Collaboration)

[1]*Dipartimento di Fisica e Astronomia "Ettore Majorana" Università di Catania Catania 95123 Italy*

[2]*Istituto Nazionale di Fisica Nucleare Laboratori Nazionali del Sud Catania 95123 Italy*

[3]*Instituto de Física Universidade Federal Fluminense Niterói 24210-346 Brazil*

[4]*Istituto Nazionale di Fisica Nucleare Sezione di Napoli Napoli 80126 Italy*

[5]*Dipartimento di Matematica e Fisica Università della Campania "Luigi Vanvitelli" Caserta 81100 Italy*

[6]*Istituto Nazionale di Fisica Nucleare Sezione di Torino Torino 10125 Italy*

[7]*Instituto de Física Universidad Nacional Autónoma de México Mexico City 04510 Mexico*

[8]*Université de Caen Normandie ENSICAEN CNRS/IN2P3 LPC Caen UMR6534 F-14000 Caen France*

[9]*Turkish Accelerator and Radiation Laboratory Ankara 06830 Turkey*

[10]*Department of Mathematics and Science Education Faculty of Education Akdeniz University 07058 Antalya Turkey*

[11]*Centro Universitario FEI São Bernardo do Campo 09850-901 Brazil*

[12]*Department of Physics Recep Tayyip Erdogan University 53100 Rize Turkey*

[13]*Instituto de Pesquisas Energeticas e Nucleares IPEN/CNEN São Paulo 05508-000 Brazil*

[14]*Instituto de Física Universidade de São Paulo São Paulo 05508-090 Brazil*

[15]*Department of Physics University of Ioannina and Hellenic Institute of Nuclear Physics Ioannina 451 10 Greece*

[16]*Department of Chemistry University of Athens and Hellenic Institute of Nuclear Physics Athens 157 84 Greece*

[17]*Department of Physics Akdeniz University 07058 Antalya Turkey*

(Received 5 September 2023; accepted 21 November 2023; published 5 January 2024)

Background: In recent years, the NUMEN project has highlighted that the systematic study of double charge exchange (DCE) nuclear reactions could provide precious information on the nuclear matrix elements of neutrinoless double β decay. To achieve this goal, a multichannel approach was adopted, where a plethora of different reaction channels is measured under the same experimental conditions and analyzed in a coherent framework. In this context, the initial (ISI) and final (FSI) state interactions are fundamental building blocks to investigate all the relevant direct nuclear reactions. To date, such building blocks are not sufficiently established for many of the projectile-target pairs of interest for NUMEN experiments. This is also the case of the $^{18}\mathrm{O} + {}^{48}\mathrm{Ti}$ system, which is relevant for the double β decay of the ^{48}Ca nucleus into the ^{48}Ti one.

Purpose: This work aims at deducing the ISI to be used in the multichannel study of the $^{18}\mathrm{O} + {}^{48}\mathrm{Ti}$ collision at 275 MeV incident energy. To this purpose, the optical potential and the strength of the couplings between elastic and inelastic scattering channels are determined and characterized by comparison with new experimental data.

Methods: Cross section angular distributions were measured for the elastic and low-lying inelastic scattering channels in a wide range of momentum transfer. Experimental data were compared to theoretical calculations performed in optical model (OM), distorted-wave Born approximation (DWBA), coupled channels (CC), and coupled channels equivalent polarization potential (CCEP) approaches. For all of them, the São Paulo double-folding potential was adopted as the optical potential. The comparison between the predictions of the OM/DWBA and CC frameworks allowed to evaluate the strength of the couplings to the inelastic channels which were explicitly taken into account. Within the CC formalism, different coupling schemes were compared to assess the contributions of the states included in the model space. A further test of our approach was carried out by analyzing the experimental data of the same system at 54 MeV incident energy.

Results: The achieved energy resolution allowed to resolve the elastic scattering and the excitation of the 2_1^+ state of the ^{48}Ti nucleus. A broad structure, associated to the superposition of the inelastic transitions to the 2_1^+ state of ^{18}O and to three excited states of ^{48}Ti, was also observed. The OM and DWBA calculations are not able to reproduce the experimental elastic and inelastic angular distributions in the explored range of momentum transfer. A significant improvement in the description of the data is found by using the CC approach. In particular,

*giuseppe.brischetto@lns.infn.it

when the 2_1^+ and 3_1^- collective states of projectile and target and their simultaneous excitations are included in the coupling scheme, a satisfactory agreement is achieved. The CCEP predictions describe reasonably well the elastic scattering data.

Conclusions: Channel coupling effects have to be taken into account for a good description of the elastic and inelastic experimental angular distributions in the measured range of momentum transfer. The inclusion of such couplings in the ISI is envisaged for the analysis of all the direct nuclear reactions induced by the $^{18}O + ^{48}Ti$ collision in this incident energy region.

DOI: 10.1103/PhysRevC.109.014604

I INTRODUCTION

The multichannel approach, recently adopted in the framework of the NUMEN (NUclear Matrix Elements for Neutrinoless double beta decay) [1,2] and NURE (NUclear REactions for neutrinoless double beta decay) [3] projects, is a promising method to describe heavy-ion induced double charge exchange (DCE) reactions, whose spectroscopy is expected to provide valuable insights into the many-body nuclear aspects involved in the neutrinoless double beta ($0\nu\beta\beta$) decay process [4,5]. Such an approach, which consists of the global analysis of a wide ensemble of nuclear reactions (including elastic and inelastic scattering, one- and two-nucleon transfers, single and double charge exchange reactions) [4,6,7], has been successfully applied to several systems of interest for NUMEN, such as ^{40}Ca [4,8,9], ^{12}C [6], ^{76}Se [10–12], ^{116}Cd [7], and ^{48}Ti [13,14]. Among them, the ^{40}Ca and ^{116}Cd cases represent concrete examples of how an approach based on quantomechanical methods (both in distorted-wave Born approximation and coupled channels formalisms), together with the São Paulo optical potential [15,16] and nuclear structure inputs derived from large-scale shell-model calculations, gives a reliable and coherent description of a plethora of reaction channels measured under the same experimental conditions.

The theoretical description of each reaction channel comprised in the multichannel network, including DCE, requires the knowledge of the initial (ISI) and final state interactions (FSI) that determine the incoming and outgoing distorted waves, respectively. The key ingredient for the ISI and the FSI is the optical potential (OP), which describes the average nucleus-nucleus potential [17,18]. Since the gateway to the OP is the study of elastic and inelastic scattering, this analysis plays a central role in the multichannel strategy proposed by NUMEN.

In the literature, many different forms for the OP have been proposed, which can be grouped into two main categories, usually referred to as phenomenological and microscopic models [19]. In the former, the OP is described with an analytic function whose radial shape mimics the nuclear density profile as a consequence of the short range of the nuclear forces. The most popular form of the phenomenological OPs is the Woods-Saxon function, whose parameters are typically obtained by fitting elastic scattering experimental cross sections (e.g., [20–23]) or from wide systematics in mass and energy [24,25]. Among the microscopic models, a considerable interest was raised by the double-folding approach (e.g., [19,26,27]), where the OP is calculated by folding an effective nucleon-nucleon interaction with the densities of projectile and target, typically assumed frozen in their ground state [17]. The use of frozen densities relies on the peripheral nature of heavy-ion direct reactions, which are expected to produce small changes in the initial states of the colliding nuclei. In our previous works, the double-folding São Paulo potential (SPP) was successfully adopted as the relevant OP. In particular, to minimize the number of free parameters, the same shape for both the real and the imaginary parts is used, the latter being scaled through a normalization factor whose value depends on the adopted coupling scheme. Elastic scattering data of light [28,29], medium [30], and heavy [31] mass nuclei suggest that angular distribution cross sections can be reasonably described by using a scaling factor of 0.78 when no couplings to excited states are accounted for, whereas 0.6 in case couplings to inelastic transitions are explicitly taken into account. This prescription was proved to be valid also for the systems investigated within the NUMEN project [6–8,10,32,33]. The analysis of such systems within the coupled channels (CC) approach highlighted that couplings to low-lying collective excitations are important at large transferred linear momenta, where the elastic scattering cross section is low and becomes comparable to inelastic scattering one [6–8,10,32,33].

The goal of this work is the experimental and theoretical analysis of the elastic and inelastic scattering in the $^{18}O + ^{48}Ti$ collision at 275 MeV incident energy as a part of the NUMEN experimental campaign. The ^{48}Ti nucleus was chosen as a target since it is the daughter of ^{48}Ca in the double β decay process. In the context of the systematic study of the $^{18}O + ^{48}Ti$ collision, the OP deduced from the present analysis has been recently adopted in the theoretical description of the ^{48}Ti(^{18}O, ^{19}F)^{47}Sc one-proton pick-up [13] and the ^{48}Ti(^{18}O, ^{17}O)^{49}Ti one-neutron stripping [14] reactions. The experimental cross section angular distributions for the elastic and two inelastic scattering transitions are presented here for the first time. Since this work mainly aims at determining the ISI for the system under investigation, theoretical calculations, adopting the SPP, are performed within different approaches and compared to the experimental data. An analysis in terms of a trivially equivalent local polarization (TELP) potential [34] is also performed, in order to derive an interaction effectively including the coupling effects, which will be employed for the study of single and double charge exchange reactions. This is motivated by the lack, to our knowledge, of suitable CC approaches able to describe such classes of reactions, which are instead analysed in terms of distorted-wave Born approximation (DWBA).

In the literature the $^{18}O + ^{48}Ti$ system was already studied by Essel and co-workers at 54 MeV incident energy [22]. This data set is herein analyzed in the same theoretical framework

as the data at 275 MeV in order to test our approach, whose ingredients are all energy independent, except for the SPP. Therefore, the experimental data at 54 MeV were considered a useful test bench to verify the reliability of our methodology at a different incident energy. This is valuable also in view of the future NUMEN experimental campaign, where it is planned to perform experiments in a wide range of incident energies [2].

This paper is organized as follows. In Sec. II the experimental setup and the experimental data are presented. Section III describes the theoretical analysis: herein, the optical model (OM), DWBA, CC, and coupled-channel equivalent polarization potential (CCEP) calculations are compared to the experimental angular distributions. In the same section, the theoretical analysis of the experimental data at 54 MeV is also discussed. The conclusions are given in Sec. IV.

II EXPERIMENTAL APPARATUS AND DATA REDUCTION

The experiment was performed at the Laboratori Nazionali del Sud of the Istituto Nazionale di Fisica Nucleare (INFN-LNS) in Catania, using an $^{18}O^{8+}$ beam accelerated at 275 MeV incident energy by the K800 superconducting cyclotron [35]. The fully stripped ions were delivered to the object point of the MAGNEX large acceptance magnetic spectrometer [36], where the target was positioned. The beam spot size and its angular divergence were reduced to 3 mm and 3 mr, respectively, by using a 2 mm diameter collimator and a 4 mm diameter antiscatterer, placed 125 and 20 mm upstream the target position, respectively. The target consisted of a 510 $\pm$ 25 μg/cm^2 thick TiO_2 layer, evaporated on a 216 $\pm$ 11 μg/cm^2 thick aluminum backing. To estimate the background contributions due to the oxygen and the aluminum target components, auxiliary measurements, under the same experimental conditions, with WO_3 + ^{27}Al and ^{27}Al targets were performed. In the energy and angular regions reported in this work, such contributions are kinematically separated from the ^{48}Ti one. A copper Faraday cup (FC) with 0.8 cm entrance diameter and 3 cm depth was placed 15 cm downstream the target position in order to stop the beam and collect the total charge in each run. A charge collection accuracy better than 10 was achieved by equipping the FC with an electron suppressor polarized at −200 V and using a low-noise charge integrator.

The ^{18}O ejectiles scattered by the target were analyzed in momentum by MAGNEX and measured by its focal plane detector (FPD) [37,38]. The experimental data were acquired in three separate data sets, where the MAGNEX optical axis (θ_{opt}) was set at 9°, 15°, and 21° with respect to the beam direction, thus covering an overall angular range from 4° to 27° in the laboratory reference frame, corresponding to the angular region between 6° and 37° in the center-of-mass (c.m.) one. In the runs with $\theta_{opt} = 15°$ and 21° the MAGNEX angular acceptance was set to its maximum value corresponding to a solid angle of 50 msr. In the configuration with $\theta_{opt} = 9°$, MAGNEX was operated in full horizontal acceptance but with a reduced vertical one, in order to have an event rate compatible with the maximum value tolerated by the FPD.

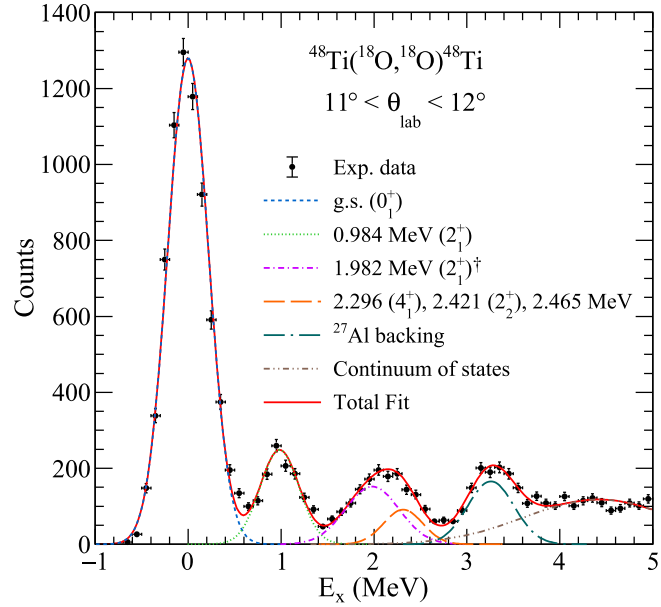

FIG. 1. Excitation energy spectrum for the ^{18}O + ^{48}Ti elastic and inelastic scattering at 275 MeV in the angular range 11° < θ_{lab} < 12°. The red solid line shows the result of the multiple-fit procedure. The other colored curves identify different states of ^{48}Ti with ^{18}O lying in its g.s., except for the curve marked by the dagger, which refers to the 2^+_1 excited state of the projectile with the target in its g.s. The structure due to the Al backing is also indicated.

The data reduction procedure adopted in the present analysis follows the prescription described in details in previous publications [39,40]. It involves the calibration of the positions measured by the FPD; the particle identification to select the $^{18}O^{8+}$ ions [41]; the reconstruction of the ejectiles trajectories to the tenth order and the extraction of the momentum vector at the target position for each event [42]. The data reduction procedure also includes the evaluation of the overall detection efficiency [43], which is a fundamental information to determine absolute differential cross sections, knowing the measured ^{18}O event yields.

The reconstruction of the momentum vector at the target position allows to determine the initial kinetic energy of the ejectiles, which, together with the scattering angle in the laboratory reference frame (θ_{lab}), is used for calculating the ejectiles excitation energy (E_x) by means of the missing mass method [44]. In Fig. 1, an example of a reconstructed excitation energy spectrum for the ^{18}O + ^{48}Ti elastic and inelastic scattering is shown. Thanks to the achieved energy resolution of $\delta E_x \approx 0.5$ MeV (FWHM), the first peak, associated to the elastic scattering, is clearly separated from the second one, which is attributed to the inelastic transition to the 2^+_1 state of ^{48}Ti at $E_x = 0\,984$ MeV. Besides the first two peaks corresponding to isolated states, a broad structure centered at about 2.2 MeV is visible. It corresponds to the superposition of the 2^+_1 excited state of the ^{18}O at 1.982 MeV and three states of ^{48}Ti nucleus: the 4^+_1 state at 2.296 MeV, the 2^+_2 state at 2.421 MeV, and a state of unknown spin-parity at 2.465 MeV [45]. The structure centered at ≈3 4 MeV is ascribed to the elastic scattering on the ^{27}Al backing of

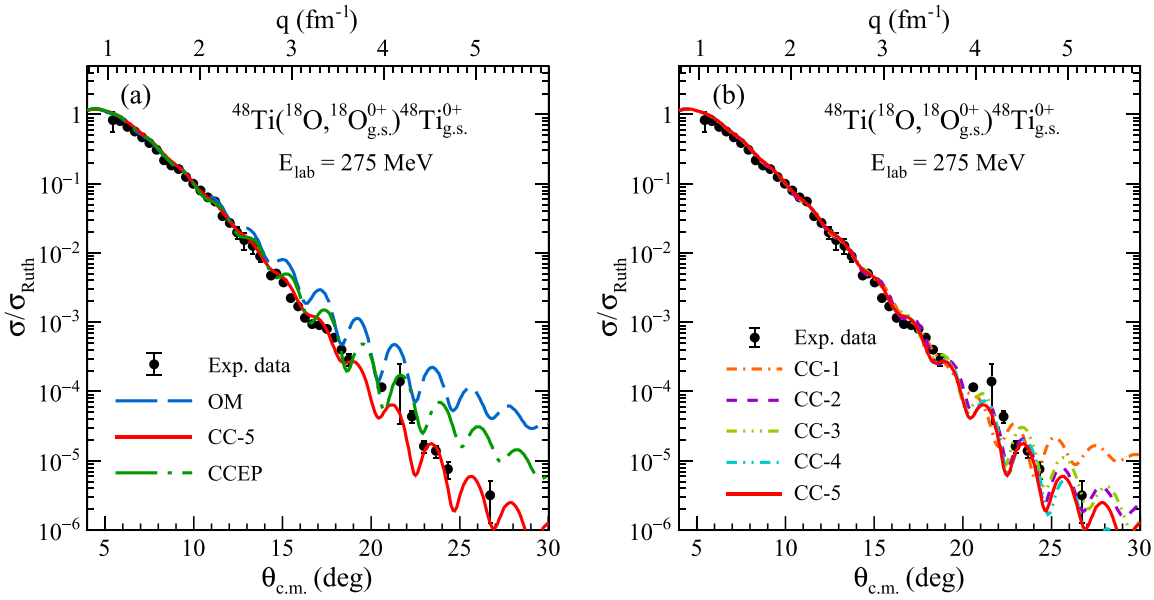

FIG. 2. Cross section angular distribution of the $^{18}O + ^{48}Ti$ elastic scattering at 275 MeV in terms of the ratio with the Rutherford one: in (a) the experimental data (black circles) and the results of the OM (blue dashed line), CC (red solid line), and CCEP (green dot-dashed line) theoretical calculations are shown. In (b) the comparison between different coupling schemes in the CC theoretical approach is illustrated (see text for details). All the theoretical curves are folded with the experimental angular resolution.

the target, while the contribution of the elastic scattering on ^{16}O is found at ≈8 5 MeV. The overall excitation energy spectrum was divided into angular slices with steps ranging from 0 3° to 4° depending on the statistics. For each angular slice, a multiple-fit procedure was carried out to interpret such a spectrum in terms of the low-lying states of ejectile and recoil nucleus, as reported in Refs. [6,10,32,33]. It was assumed that each observed peak may be approximated to a Gaussian function. The width of each Gaussian function was fixed according to the FWHM of the $^{48}Ti(2^+_1)$ inelastic peak; for the inelastic transitions populating bound excited states of the ^{18}O, the Doppler broadening due to the in-flight γ decay of the ejectiles was also taken into account. The experimental yield of each transition was deduced from the area of the corresponding Gaussian function.

The elastic cross section angular distribution in terms of its ratio to the Rutherford one is shown in Fig. 2 as a function of the scattering angle ($\theta_{c\,m}$) in the c.m. reference frame. The error bars include contributions from the statistical error, the fitting procedure, and the solid angle evaluation. The systematic error due to uncertainties in the measurement of the total charge and in the evaluation of the target thickness was estimated to be less than 10 and it is not explicitly considered in the error bars, since it is common to all the experimental points. A representation in terms of the linear momentum transfer $\vec{q} = \vec{k}_n - \vec{k}_0$ is also given with $\vec{k}_0$ and $\vec{k}_n$ the linear momenta in the initial and final state, respectively. Since for elastic scattering $|\vec{k}_n| = |\vec{k}_0|$, the modulus of the momentum transfer can be expressed as

$$q = \frac{2\sqrt{2\mu c^2 E_{c\,m}}}{\hbar c} \sin\frac{\theta_{c\,m}}{2}, \qquad (1)$$

where μ is the reduced mass for the colliding nuclei and $E_{c\,m}$ is the energy in the c.m. reference frame. The three data sets ($\theta_{opt} = 9°$, 15°, and 21°) were found to be in good agreement with each other without the need of any renormalization factor, pointing out an accurate measurement of the detection efficiency. The experimental data show the typical Fresnel-like diffraction pattern, as expected for heavy-ion elastic scattering at energies above the Coulomb barrier (Sommerfeld parameter ≈7). Up to the grazing angle ($\theta_{gr} \approx 7\,6°$ in the c.m. reference frame), the scattering is expected to be mainly driven by the Coulomb field. Beyond such angle, the nuclear part of the interaction potential becomes dominant, giving rise to strong absorption phenomena manifested as a sharp decrease of the elastic cross section. This characteristic fall-off of the elastic scattering angular distribution is usually interpreted in terms of the near-side scattering amplitudes [17].

The experimental cross section angular distributions for the $^{48}Ti(2^+_1)$ transition ($E_x = 0\,984$ MeV) and for the structure centered at 2.2 MeV are shown in Figs. 3 and 4, respectively. In both cases, the linear momentum transfer scale is also reported. Both the angular distributions exhibit an oscillatory behavior up to $\theta_{c\,m} \approx 18°$ which is more pronounced in the case of the target excitation.

III THEORETICAL ANALYSIS

A theoretical description of the elastic and inelastic scattering experimental data is fundamental to deduce the ISI to be used in the multichannel approach of the nuclear reactions network induced by the $^{18}O + ^{48}Ti$ collision at the same incident energy. The ISI is responsible for the distortion of the incoming waves, therefore it is essential to properly describe all the direct nuclear reaction channels. The theoretical

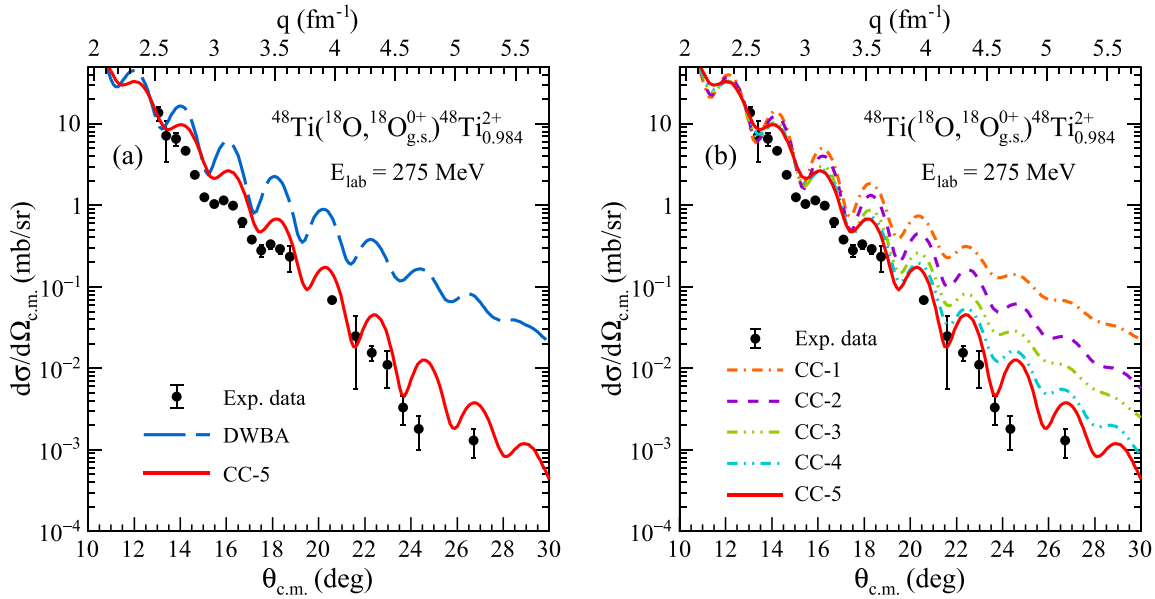

FIG. 3. Cross section angular distribution of the inelastic scattering to the 2^+_1 excited state of the ^{48}Ti at 0.984 MeV: in (a) the experimental data (black circles) and the results of the DWBA (blue dashed line) and CC (red solid line) theoretical calculations are shown. In (b) the comparison between different coupling schemes in the CC theoretical approach is illustrated (see text for details). All the theoretical curves are folded with the experimental angular resolution.

calculations for the elastic and inelastic scattering were performed in OM, DWBA, CC, and CCEP formalisms. All calculations were performed by using the FRESCO code [46].

In the OM framework, the complicated many-body problem of the interaction between two nuclei is simplified into that of a particle scattered by a nonlocal complex potential, called OP [17,18]. In many cases, OPs are taken to be local, where the nonlocality effects are treated in terms of an energy dependence: they are usually referred to as *local-equivalent* potentials [17]. The local-equivalent OP $U_{\rm opt}(r)$ may be

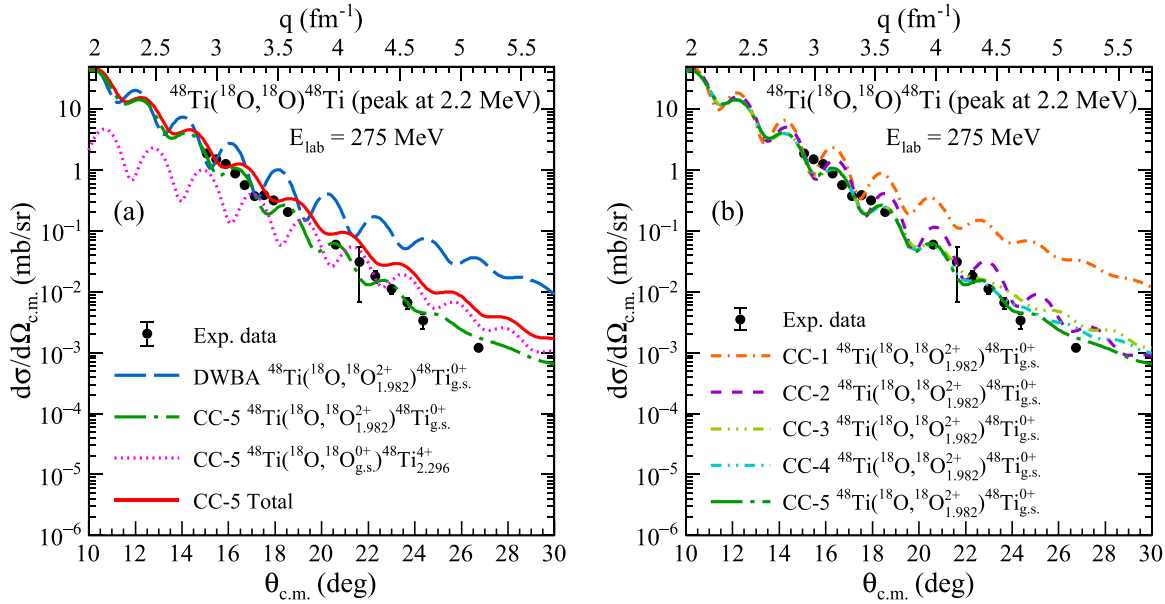

FIG. 4. Cross section angular distribution of the structure centered at 2.2 MeV in the excitation energy spectrum of Fig. 1. In (a) the experimental data (black circles) are shown, together with the results of the DWBA (blue dashed line) and CC (green dot-dashed line) theoretical calculations for the inelastic excitation of the 2^+_1 state of ^{18}O at 1.982 MeV. The CC prediction for the scattering to the 4^+_1 excited state of ^{48}Ti is reported (magenta dotted line). The sum of the two transitions, as calculated within the CC framework, is indicated by the red solid line. In (b) the comparison between different coupling schemes for the CC calculation of the transition to the 2^+_1 state of ^{18}O is presented (see text for details). All the theoretical curves are folded with the experimental angular resolution.

written as the sum of a real $V(r)$ and an imaginary $W(r)$ part:

$$U_{\rm opt}(r) = V(r) + iW(r), \tag{2}$$

where r is the distance between the centers of mass of two colliding nuclei. While the real part of the OP accounts for the refraction of the incident waves, the imaginary term is introduced to describe the absorption effects leading to a loss of flux from the elastic process towards nonelastic channels not explicitly included in the model space.

In the double-folding framework, the real part $V(r)$ of the nuclear potential is constructed as the integral of the nucleon-nucleon effective interaction $V_{NN}(r_{12}, E_N)$ weighted by the ground-state matter density distributions $\rho_1(\mathbf{r}_1)$ and $\rho_2(\mathbf{r}_2)$ of projectile and target, respectively. It may be expressed as

$$V(r) = \iint d\mathbf{r}_1 d\mathbf{r}_2\, \rho_1(\mathbf{r}_1)\, \rho_2(\mathbf{r}_2)\, V_{NN}(r_{12}, E_N), \tag{3}$$

where $r_{12} = |\mathbf{r} - \mathbf{r}_1 + \mathbf{r}_2|$, $\mathbf{r}_1$ and $\mathbf{r}_2$ represent the internal coordinates of the two nuclei, and E_N is the energy per nucleon in the c.m. reference frame.

The OP adopted in this work is the double-folding local-equivalent São Paulo potential (SPP) $V_{\rm SPP}$ [15], which can be expressed as follows:

$$V_{\rm SPP}(r) = V(r)\, e^{-\frac{4}{c^2}}, \tag{4}$$

where $V(r)$ is given by Eq. (3), is the velocity between projectile and target and c is the speed of light. The exponential factor in Eq. (4) is the Pauli nonlocality term [15]. In this analysis, the SPP was used for both the real and the imaginary parts of the OP, according to

$$U_{\rm opt}(r) = (N_V + iN_W)\, V_{\rm SPP}(r), \tag{5}$$

where N_V and N_W are normalization factors for the real and imaginary parts, respectively. The adopted values for N_V and N_W derive from a wide systematics, where the SPP was used to describe experimental data [6,7,10,28,30–33,47–50]. Based on such a systematics, for energies above the Coulomb barrier, N_V is set to 1, while the value of N_W depends on the coupling scheme adopted in the calculations. In the OM approach, where only the elastic channel is considered in the model space (for this reason it is also known as one-channel approximation), N_W is typically set to 0.78. The same holds also for the DWBA framework used to describe reaction channels; on the contrary, when the couplings to the inelastic transitions towards the low-lying collective states are explicitly taken into account in the CC approach, the N_W value is typically decreased to 0.6 [16].

The matter densities $\rho_j(\mathbf{r}_j)$ adopted in the double-folding procedure of the SPP are two-parameters (radius R and diffuseness a) Fermi distributions and are assumed to be spherical. The radius and diffuseness adopted in the present analysis are taken from the systematic analysis of electron scattering data and Dirac-Hartree-Bogoliubov calculations for a wide range of nuclei [15]. In the specific case of the ^{18}O, a diffuseness of 0.61 fm was adopted, which is larger by a 10 with respect to the value reported in the SPP systematics. This assumption, explored in details in several publications [8,10,29,51–53], accounts for the effects of the two valence neutrons orbiting around the ^{16}O core in the ^{18}O ground state. Some relevant properties of the adopted SPP, such as the volume integral per nucleon J and the total reaction cross section σ_R, are reported in Table I.

TABLE I. Coefficient of the imaginary part of the SPP (N_W), volume integral per nucleon for the real (J_V) and the imaginary (J_W) part of the SPP, and total reaction cross section σ_R in the case of the OM/DWBA, CC, and CCEP calculations.

Theor. approach	N_W	J_V (MeV fm^3)	J_W (MeV fm^3)	σ_R (mb)
OM/DWBA	0.78	−346	−270	2571
CC	0.60	−346	−208	2498
CCEP	1.0	−247	−176	2480

A Analysis of the data at 275 MeV incident energy

The comparison between the predictions of the OM calculation and the elastic scattering angular distribution for the experimental data at 275 MeV incident energy is shown in Fig. 2(a). A good agreement can be noticed up to $\theta_{\rm c\,m} \approx 13^\circ$, corresponding to a linear momentum transfer $q \approx 2\ 5$ fm^{-1}, while at larger scattering angles the OM calculation overestimates the experimental data. Such a discrepancy arises since at large momentum transfer the cross sections of nonelastic channels become comparable with the elastic scattering one, so that the couplings to the first low-lying inelastic excitations must be explicitly taken into account for a better description of the data, as observed in similar analysis [6,10,32,33]. To this extent, CC calculations were performed and are presented in the following. In this work, the first low-lying excited states of both projectile (2^+_1 and 3^-_1) and target (2^+_1, 3^-_1, and 4^+_1) are considered in the coupling scheme, as sketched in Fig. 5, and treated as collective excitations within the rotational model. In the DWBA approach the second-order transitions to the simultaneous excitations of projectile and target are not included because in such an approach only first-order processes are allowed. For the same reason, the back-coupling to the elastic channel is not allowed in DWBA. In the macroscopic model adopted in this work, the coupling potentials are derived from the multipole expansion of the OP [17,54]. Quadrupole and octupole ($\lambda = 2, 3$) excitations of the deformed ^{18}O and ^{48}Ti nuclei are taken into account and the coupling potentials include both the Coulomb and the nuclear components. The Coulomb coupling potential $V_C(r, \lambda)$ for the λ-multipolarity is defined as follows:

$$V_C(r, \lambda) = M(E\lambda)\, \frac{\sqrt{4\pi}}{2\lambda + 1}\, r^{-\lambda-1}, \tag{6}$$

where $M(E\lambda)$ is the matrix element of the electric multipole operator $E\lambda$. The quantity $M(E\lambda)$ can be related to the reduced transition probability $B(E\lambda; J \quad J')$ from the initial state J to the final one J' through the $E\lambda$ operator, according to

$$M(E\lambda) = \pm\sqrt{(2J+1)B(E\lambda; J \quad J')} \tag{7}$$

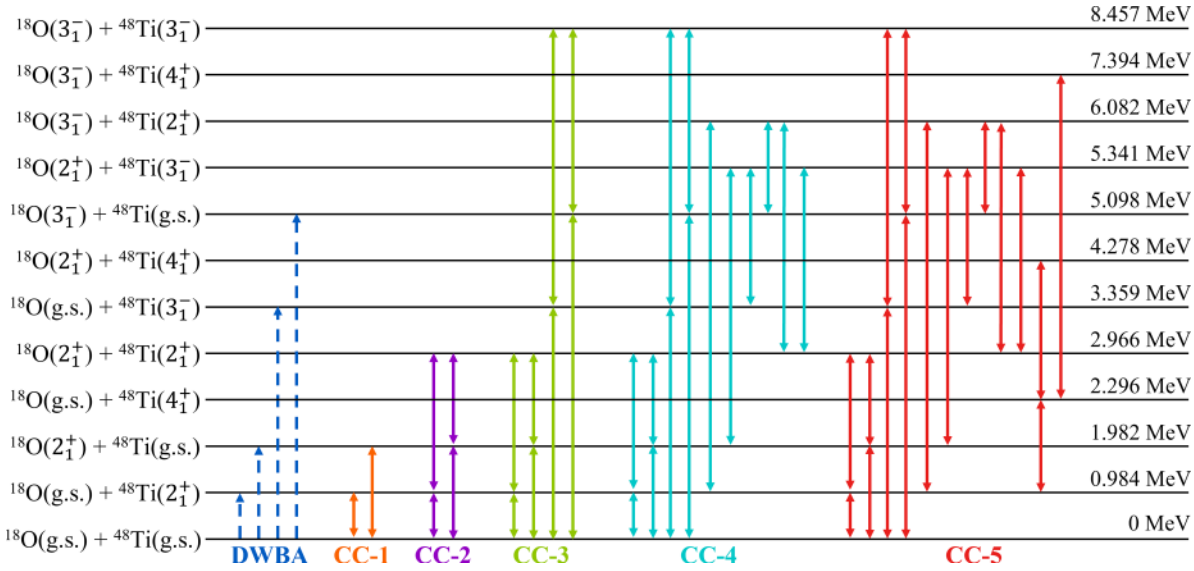

FIG. 5. Coupling schemes adopted for the DWBA and CC theoretical calculations of the ^{18}O + ^{48}Ti elastic and inelastic scattering at 275 MeV incident energy. On the right, the excitation energies of the considered states are reported.

As indicated in Ref. [46], the sign of the $M(E\lambda)$ is the same as the intrinsic quadrupole moment (Q_0). The nuclear coupling potentials $V_N(r, \lambda)$ are usually described in terms of deformations of the OP and approximated as

$$V_N(r, \lambda) = -\frac{\delta_\lambda}{\sqrt{4\pi}} \frac{dU_{\rm opt}(r)}{dr}, \tag{8}$$

where δ_λ is the deformation length, accounting for the strength of the coupling. Under the assumption that the deformation length of the mass distribution is equal to the charge distribution one, δ_λ can be related to $M(E_\lambda)$ according to

$$\delta_\lambda = \beta_\lambda R_V = \frac{4\pi}{3Ze} \frac{M(E\lambda)}{R_V^{\lambda-1}}, \tag{9}$$

in which β_λ is the deformation parameter for the 2^λ transition, Z is the atomic number of the nucleus, e is the electron charge, and R_V is the average radius of the SPP, expressed as

$$R_V = \frac{dr\, 4\pi r^3 V(r)}{dr\, 4\pi r^2 V(r)} \tag{10}$$

The same prescriptions for the Coulomb and nuclear coupling potentials were used in some recent papers [8–11,13,33].

For the mentioned ingredients, we decided to adopt the experimental values reported in the literature [55–57], which are listed in Table II. In addition, a large-scale shell-model calculation was performed by using the KSHELL code [58], adopting the same interactions as in Ref. [13]. As one can see in Table II, the theoretical $M(E\lambda)$ values are found to be in a reasonably good agreement with the experimental ones for all the transitions.

The DWBA prediction for the ^{48}Ti(2^+_1) inelastic transition is compared to the measured angular distribution in Fig. 3(a), where it can be noticed that the calculation fails to reproduce the behavior of the experimental data, especially at large angles, where the effects of channel couplings are expected to be more relevant. A similar result is obtained also by looking at Fig. 4(a), in which the comparison between the angular distribution of the structure centered at 2.2 MeV and the DWBA calculation for the ^{18}O(2^+_1) excitation is shown. It is worth to remark that also the inelastic transitions to the excited states at 2.296 MeV (4^+_1), 2.421 MeV (2^+_2), and 2.465 MeV (unknown spin-parity) of ^{48}Ti are expected to contribute to the cross section of the structure centered at 2.2 MeV. In the one-step DWBA approach, it is not possible to account for

TABLE II. Adopted values of average radius R_V of the SPP, experimental reduced transition probability $B(E\lambda; J \quad J')_{\rm exp}$, reduced matrix element $M(E\lambda)_{\rm exp}$, and deformation length $\delta_\lambda^{\rm exp}$ for $\lambda = 2$, 3 for the ^{18}O and ^{48}Ti nuclei. The reduced matrix elements computed with the KSHELL code [58] ($M(E\lambda)_{\rm theo}$) are also reported.

	R_V (fm)	$B(E2; 0^+ \quad 2^+)_{\rm exp}$ (e^2fm^4)	$M(E2)_{\rm exp}$ (e fm^2)	$M(E2)_{\rm theo}$ (e fm^2)	$\delta_2^{\rm exp}$ (fm)	$B(E3; 0^+ \quad 3^-)_{\rm exp}$ (e^2 fm ^{6})	$M(E3)_{\rm exp}$ (e fm^3)	$M(E3)_{\rm theo}$ (e fm ^{3})	$\delta_3^{\rm exp}$ (fm)
^{18}O	4.60	43[a]	+6.56	+5.18	+0.75	1300[b]	+35.36	+36.15	+0.87
^{48}Ti		720[c]	+26.83	+22.46	+1.11	7400[b]	+75.25	+75.28	+0.77

[a]From Ref. [55].
[b]From Ref. [56].
[c]From Ref. [57].

such transitions since they are populated through second-order processes.

Regarding the CC approach, five different coupling schemes were investigated with the aim to evaluate the strength of the couplings to different excited states of projectile and target. Such coupling schemes, which are referred to as CC-1, CC-2, etc., are shown in Fig. 5. In Fig. 2(b), the comparison between the CC calculations with the different coupling schemes is reported for the elastic scattering case. For all the coupling schemes the CC calculations are in reasonable agreement with the experimental data up to $\theta_{c\,m} \approx 22^\circ$, but at larger scattering angles CC-1 is not able to reproduce the magnitude of the angular distribution. A remarkable improvement in the description of the experimental data is obtained when the $^{18}O(2_1^+) + {}^{48}Ti(2_1^+)$ transition is introduced in the model space (CC-2, CC-3, CC-4, and CC-5 models). In particular, when the CC-5 coupling scheme is adopted, a fair agreement between CC calculations and the experimental angular distribution is reached.

In the case of the inelastic transition to the 2_1^+ state of ^{48}Ti, each successive enlargement of the coupling scheme produces a significant impact on the theoretical angular distribution, so that the optimum description of the experimental data is obtained when the CC-5 coupling scheme is considered [see Fig. 3(b)]. However, even with such a coupling scheme a discrepancy by a factor of about 2 between theoretical calculations and experimental data is present, maybe calling for an even broader model space.

In Fig. 4(b), the angular distribution of the structure centered at 2.2 MeV is compared to the CC predictions for the $^{18}O(2_1^+)$ inelastic excitation. Analogously to the elastic scattering case, the inclusion of the 2_1^+ simultaneous excitation of projectile and target improves considerably the agreement between theoretical predictions and experimental data. As mentioned before, it is expected that other inelastic transitions contribute to the cross section of the structure centered at 2.2 MeV. Within the CC framework, we calculated the contribution of the $^{48}Ti(4_1^+)$ transition and we found that it is comparable with the 2_1^+ excitation of ^{18}O [see Fig. 4(a)]. The sum of the CC predictions for the $^{18}O(2_1^+)$ and $^{48}Ti(4_1^+)$ transitions is compared to the experimental data in Fig. 4(a), where it can be observed that the theoretical angular distribution overestimates the experimental one at larger scattering angles.

The substantial difference between DWBA and CC calculations observed in the elastic scattering and in both the inelastic transitions is a clear sign of the importance of the couplings, especially at large momentum transfer. Therefore, the same couplings should be taken into account in the ISI used for the description of the other direct reaction channels populated by the same projectile and target at the same incident energy [14]. Nonetheless, the high-order effects included in the CC calculations are expected to be relevant when there is a strong channel coupling (e.g., between the low-lying collective excitations and the elastic scattering channel), while for reaction channels that are weakly coupled to such collective states (like single charge exchange reactions) a first-order DWBA may be sufficient [8]. A specific investigation of this point is beyond the scope of this article and it deserves a detailed analysis. In addition, the explicit introduction of the couplings in theoretical calculations of complex reaction channels can be demanding from the computational point of view.

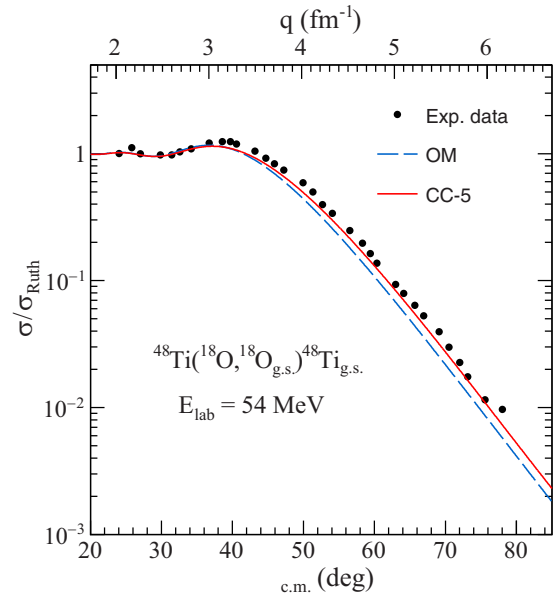

FIG. 6. Experimental cross section angular distribution of $^{18}O + {}^{48}Ti$ elastic scattering at 54 MeV in terms of the ratio with the Rutherford cross section [22]. The OM and CC theoretical calculations are also shown with the blue dashed and the red solid lines, respectively.

For this reason, the effects of channel couplings were incorporated in the OP by means of an effective polarization potential term, as described in Ref. [34]. In particular, we used a local L-independent polarization potential, usually referred to as *trivially equivalent local polarization* (TELP) potential. The effective potential resulting from the sum between the TELP obtained with the CC-5 coupling scheme and the bare SPP used for the CC analysis was employed to perform CCEP calculations for the elastic scattering channel. The predictions of such calculations are shown in Fig. 2(a), where it can be noticed that the CCEP approach describes well the experimental data up to ≈ 4 fm^{-1}. At larger momentum transfers, it overestimates the measured angular distribution, being somehow in an intermediate condition between the OM and the CC predictions. This seems to be reasonable since in the CCEP framework the coupling effects are accounted for on average and, therefore, it is not able to reproduce the experimental data in the region of high momentum transfer, where the influence of couplings is stronger.

B Analysis of the data at 54 MeV incident energy

As a further test of the validity of our approach, a theoretical analysis of the experimental data reported in Ref. [22] by Essel *et al.*, concerning the $^{18}O + {}^{48}Ti$ system at 54 MeV incident energy, is performed adopting the reaction framework presented above.

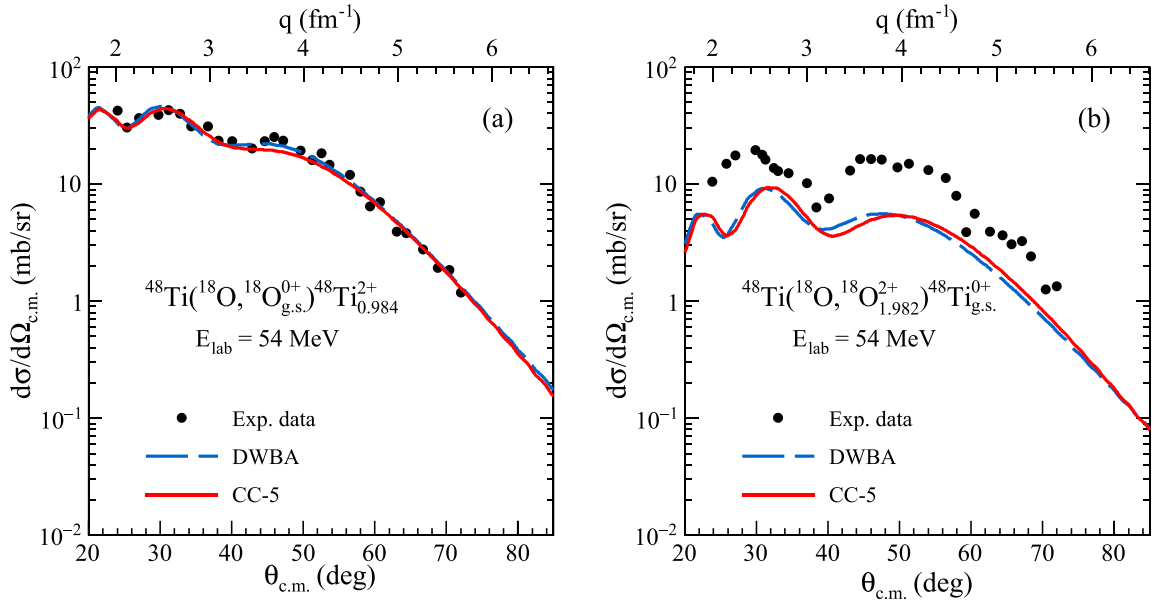

FIG. 7. Angular distributions of differential cross section for the inelastic transitions towards the 2^+_1 states of (a) ^{48}Ti and (b) ^{18}O induced by the ^{18}O + ^{48}Ti collision at 54 MeV [22]. The DWBA and CC calculations are also shown with the blue dashed and the red solid lines, respectively.

The comparison between the experimental elastic angular distribution and the corresponding OM and CC calculations is shown in Fig. 6. The experimental data, characterized by the typical Fresnel-like pattern, are well reproduced by the CC method.

The angular distributions of the inelastic transitions populating the 2^+_1 states of ^{18}O and ^{48}Ti nuclei are also analysed. Both angular distributions are compared to DWBA and CC calculations in Fig. 7. As can be noticed, for the inelastic transition towards the 2^+_1 state of the target, both calculations are in very good agreement with the experimental data; in particular, the DWBA result is compatible with the one reported in Ref. [22], where the parameters of the optical potential were deduced from a fit of the elastic scattering cross section. Instead, for the excitation of the 2^+_1 state of the projectile the calculations underestimate the experimental data. Also in Ref. [22] a disagreement is noticed. Further investigations from both the experimental and theoretical side are desirable in order to resolve the observed discrepancies.

For the three analyzed angular distributions, the calculations with and without the couplings (i.e., CC vs. OM for the elastic scattering process and CC vs. DWBA for the inelastic transitions) produce quite similar results. Therefore, it can be deduced that the coupling effects for collisions near the Coulomb barrier are less relevant.

IV CONCLUSIONS

In this work, new data for the elastic and inelastic scattering of the ^{18}O + ^{48}Ti system at 275 MeV incident energy are reported. The large acceptance of MAGNEX allowed to explore a wide range of transferred momenta in only three angular settings. Cross section angular distributions were measured for the elastic scattering, for the inelastic transition to the 2^+_1 state of ^{48}Ti, and for a structure containing the inelastic scattering to the 2^+_1 state of ^{18}O and three transitions to excited states of ^{48}Ti.

The experimental results were compared with cross-section calculations performed using the FRESCO program. The SPP was adopted as the optical potential and the couplings with the low-lying collective excited states of projectile and target were treated in terms of deformed Coulomb and nuclear potentials. The theoretical calculations were performed in OM, DWBA, CC, and CCEP approaches. The OM calculation fails to reproduce the elastic scattering experimental data at large momentum transfer. Different coupling schemes were investigated within the CC formalism. An important role of the simultaneous 2^+_1 excitation of projectile and target was observed, especially for the angular distributions of the elastic scattering and of the structure centered at 2.2 MeV. A satisfactory description of the data is obtained over the full explored angular range with the CC approach when the 2^+_1 and 3^-_1 states of projectile and target and their simultaneous excitations are included in the coupling scheme. Such a result highlights the importance of the couplings to the 2^+ and 3^- low-lying collective states of projectile and target at 275 MeV incident energy, i.e. well-above the Coulomb barrier. This is also confirmed by the analysis of the inelastic transitions, where the CC calculations reproduce the experimental data significantly better than the DWBA ones. In the light of this result, further coupled-channel Born approximation (CCBA) calculations about the one-proton pick-up reaction were performed, by taking into account the relevant couplings deduced from the present work. In the region of the experimental data, such calculations do not show any appreciable difference compared to the one reported in Ref. [13]. Regarding the inelastic excitation of the ^{48}Ti(2^+_1) state, the theoretical calculations overestimate the experimental data by a factor of about 2. In order to

evaluate the possible effects of this discrepancy in the one-proton [13] and one-neutron [14] transfer analyses, tentative CCBA calculations were performed adopting a $B(E2)$ value which was scaled to reproduce the ^{48}Ti(2_1^+) inelastic scattering data. The new results were found to be practically the same as the previous ones.

The CCEP approach, that includes the effects of channel couplings in an effective way, is in reasonable agreement with the elastic scattering angular distribution, providing a description which is better than the OM but not as accurate as CC predictions.

The validity of our approach was further tested by studying previously reported data at 54 MeV adopting the same analysis method. For the elastic transition, CC calculation gives a better description of the experimental data than the OM. For the inelastic transition to the 2_1^+ excited state of ^{48}Ti both the DWBA and CC formalisms well reproduce the data, showing a less pronounced role of the couplings to inelastic excitations at energies close to the Coulomb barrier.

The ISI determined in this work for the $^{18}\mathrm{O} + {}^{48}\mathrm{Ti}$ system is crucial for the analysis of all the other direct reactions induced at the same incident energy. The significant role of the couplings to the low-lying collective states highlights the need of exploring the effects of channel couplings also in the other reaction channels of interest for NUMEN. The inclusion of inelastic couplings in transfer reaction channels is rather under control adopting the well-established CCBA and coupled reaction channels models. The possibility of introducing such couplings also in more advanced calculations, like the case of single and double charge exchange reactions, is currently under investigation. In this context, the deduction of the TELP is valuable for the completion of such advanced theoretical calculations, since it allows to effectively account for coupling channel effects.

ACKNOWLEDGMENTS

This project received funding from the European Research Council (ERC) under the European Union's Horizon 2020 Research and Innovation Programme (Grant Agreement No. 714625). The NUMEN project is mainly funded by INFN. Support from the Brazilian funding agencies FAPESP, Proc. No. 2019/07767-1, and INCT-FNA, Proc. No. 464898/2014-5, is acknowledged. The Mexican authors received funding from DGAPA-UNAM IN107820, IG101120, and CONACYT315839 projects.

[1] F. Cappuzzello, C. Agodi, M. Cavallaro, D. Carbone, S. Tudisco, D. Lo Presti, J. Oliveira, P. Finocchiaro, M. Colonna, D. Rifuggiato, L. Calabretta, D. Calvo, L. Pandola, L. Acosta, N. Auerbach, J. Bellone, R. Bijker, D. Bonanno, D. Bongiovanni, T. Borello-Lewin *et al.*, The NUMEN project: NUclear Matrix Elements for Neutrinoless double beta decay, Eur. Phys. J. A **54**, 72 (2018).

[2] F. Cappuzzello, C. Agodi, L. Calabretta, D. Calvo, D. Carbone, M. Cavallaro, M. Colonna, P. Finocchiaro, F. Iazzi, R. Linares, J. R. B. Oliveira, L. Pandola, E. Santopinto, D. Torresi, S. Tudisco, L. Acosta, C. Altana, P. Amador-Valenzuela, L. H. Avanzi, J. Bellone *et al.*, The NUMEN technical design report, Int. J. Mod. Phys. A **36**, 2130018 (2021).

[3] M. Cavallaro, E. Aciksoz, L. Acosta, C. Agodi, N. Auerbach, J. Bellone, R. Bijker, S. Bianco, D. Bonanno, D. Bongiovanni, T. Borello-Lewin, I. Boztosun, V. Branchina, M. P. Bussa, L. Busso, S. Calabrese, L. Calabretta, A. Calanna, D. Calvo, F. Cappuzzello *et al.*, NURE: An ERC project to study nuclear reactions for neutrinoless double beta decay, PoS **302**, 015 (2017).

[4] F. Cappuzzello, H. Lenske, M. Cavallaro, C. Agodi, N. Auerbach, J. Bellone, R. Bijker, S. Burrello, S. Calabrese, D. Carbone, M. Colonna, G. De Gregorio, J. Ferreira, D. Gambacurta, H. García-Tecocoatzi, A. Gargano, J. Lay, R. Linares, J. Lubian, E. Santopinto *et al.*, Shedding light on nuclear aspects of neutrinoless double beta decay by heavy-ion double charge exchange reactions, Prog. Part. Nucl. Phys. **128**, 103999 (2023).

[5] H. Lenske, F. Cappuzzello, M. Cavallaro, and M. Colonna, Heavy ion charge exchange reactions as probes for nuclear β-decay, Prog. Part. Nucl. Phys. **109**, 103716 (2019).

[6] A. Spatafora, D. Carbone, F. Cappuzzello, M. Cavallaro, L. Acosta, C. Agodi, P. Amador-Valenzuela, T. Borello-Lewin, G. A. Brischetto, S. Calabrese, D. Calvo, V. Capirossi, E. R. Chávez Lomelí, I. Ciraldo, G. De Gregorio, F. Delaunay, H. Djapo, C. Eke, P. Finocchiaro, S. Firat *et al.* (NUMEN Collaboration), Multichannel experimental and theoretical approach to the ^{12}C(^{18}O, ^{18}F)^{12}B single-charge-exchange reaction at 275 MeV: Initial-state interaction and single-particle properties of nuclear wave functions, Phys. Rev. C **107**, 024605 (2023).

[7] S. Burrello, S. Calabrese, F. Cappuzzello, D. Carbone, M. Cavallaro, M. Colonna, J. A. Lay, H. Lenske, C. Agodi, J. L. Ferreira, S. Firat, A. Hacisalihoglu, L. La Fauci, A. Spatafora, L. Acosta, J. I. Bellone, T. Borello-Lewin, I. Boztosun, G. A. Brischetto, D. Calvo *et al.* (NUMEN Collaboration), Multichannel experimental and theoretical constraints for the ^{116}Cd(^{20}Ne, ^{20}F)^{116}In charge exchange reaction at 306 MeV, Phys. Rev. C **105**, 024616 (2022).

[8] M. Cavallaro, J. I. Bellone, S. Calabrese, C. Agodi, S. Burrello, F. Cappuzzello, D. Carbone, M. Colonna, N. Deshmukh, H. Lenske, A. Spatafora, L. Acosta, P. Amador-Valenzuela, T. Borello-Lewin, G. A. Brischetto, D. Calvo, V. Capirossi, E. Chávez, I. Ciraldo, M. Cutuli *et al.*, A constrained analysis of the ^{40}Ca(^{18}O, ^{18}F)^{40}K direct charge exchange reaction mechanism at 275 MeV, Front. Astron. Space Sci. **8**, 659815 (2021).

[9] S. Calabrese, M. Cavallaro, D. Carbone, F. Cappuzzello, C. Agodi, S. Burrello, G. De Gregorio, J. L. Ferreira, A. Gargano, O. Sgouros, L. Acosta, P. Amador-Valenzuela, J. I. Bellone, T. Borello-Lewin, G. A. Brischetto, D. Calvo, V. Capirossi, E. R. Chàvez Lomelì, I. Ciraldo, M. Colonna *et al.* (NUMEN Collaboration), ^{18}O-induced single-nucleon transfer reactions on ^{40}Ca at 15 3a MeV within a multichannel analysis, Phys. Rev. C **104**, 064609 (2021).

[10] L. La Fauci, A. Spatafora, F. Cappuzzello, C. Agodi, D. Carbone, M. Cavallaro, J. Lubian, L. Acosta, P. Amador-Valenzuela, T. Borello-Lewin, G. A. Brischetto, S. Calabrese,

D. Calvo, V. Capirossi, E. R. Chàvez Lomelí, I. Ciraldo, M. Cutuli, F. Delaunay, H. Djapo, C. Eke *et al.* (NUMEN Collaboration), $^{18}O + ^{76}Se$ elastic and inelastic scattering at 275 MeV, Phys. Rev. C **104**, 054610 (2021).

[11] I. Ciraldo, F. Cappuzzello, M. Cavallaro, D. Carbone, S. Burrello, A. Spatafora, A. Gargano, G. De Gregorio, R. I. M. n. Vsevolodovna, L. Acosta, C. Agodi, P. Amador-Valenzuela, T. Borello-Lewin, G. A. Brischetto, S. Calabrese, D. Calvo, V. Capirossi, E. R. C. Lomelí, M. Colonna, F. Delaunay *et al.* (For the NUMEN Collaboration), Analysis of the one-neutron transfer reaction in $^{18}O + ^{76}Se$ collisions at 275 MeV, Phys. Rev. C **105**, 044607 (2022).

[12] I. Ciraldo *et al.* [Phys. Rev. C (to be published)].

[13] O. Sgouros, M. Cavallaro, F. Cappuzzello, D. Carbone, C. Agodi, A. Gargano, G. De Gregorio, C. Altana, G. A. Brischetto, S. Burrello, S. Calabrese, D. Calvo, V. Capirossi, E. R. Chávez Lomelí, I. Ciraldo, M. Cutuli, F. Delaunay, H. Djapo, C. Eke, P. Finocchiaro *et al.* (for the NUMEN Collaboration), One-proton transfer reaction for the $^{18}O + ^{48}Ti$ system at 275 MeV, Phys. Rev. C **104**, 034617 (2021).

[14] O. Sgouros, M. Cutuli, F. Cappuzzello, M. Cavallaro, D. Carbone, C. Agodi, G. De Gregorio, A. Gargano, R. Linares, G. A. Brischetto, D. Calvo, E. R. Chávez Lomelí, I. Ciraldo, F. Delaunay, H. Djapo, C. Eke, P. Finocchiaro, M. Fisichella, M. A. Guazzelli, A. Hacisalihoglu *et al.* (for the NUMEN Collaboration), One-neutron transfer reaction in the $^{18}O + ^{48}Ti$ collision at 275 MeV, Phys. Rev. C **108**, 044611 (2023).

[15] L. C. Chamon, B. V. Carlson, L. R. Gasques, D. Pereira, C. De Conti, M. A. G. Alvarez, M. S. Hussein, M. A. Candido Ribeiro, E. S. Rossi, Jr., and C. P. Silva, Toward a global description of the nucleus-nucleus interaction, Phys. Rev. C **66**, 014610 (2002).

[16] D. Pereira, J. Lubian, J. R. B. Oliveira, D. P. de Sousa, and L. C. Chamon, An imaginary potential with universal normalization for dissipative processes in heavy-ion reactions, Phys. Lett. B **670**, 330 (2009).

[17] G. R. Satchler, *Direct Nuclear Reactions*, Introductory Series of Monographs on Physics, Vol. 68 (Clarendon Press, Oxford, 1983).

[18] P. E. Hodgson, The nuclear optical model, Rep. Prog. Phys. **34**, 765 (1971).

[19] G. Satchler and W. Love, Folding model potentials from realistic interactions for heavy-ion scattering, Phys. Rep. **55**, 183 (1979).

[20] T. Udagawa, T. Tamura, and B. T. Kim, Simultaneous analyses of elastic scattering and fusion cross sections for the $^{32}S + ^{58,64}Ni$ systems at energies near the Coulomb barrier, Phys. Rev. C **39**, 1840 (1989).

[21] W. Henning, Y. Eisen, J. R. Erskine, D. G. Kovar, and B. Zeidman, Optical-model potential in single-nucleon-transfer reactions induced by heavy ions, Phys. Rev. C **15**, 292 (1977).

[22] H. Essel, K. E. Rehm, H. Bohn, H. J. Körner, and H. Spieler, Inelastic scattering of ^{18}O and ^{17}O ions from medium-weight nuclei, Phys. Rev. C **19**, 2224 (1979).

[23] E. Vardaci, P. Rath, M. Mazzocco, A. D. Nitto, G. L. Rana, C. Parascandolo, D. Pierroutsakou, M. Romoli, A. Boiano, A. Vanzanella, M. Cinausero, G. Prete, N. Gelli, F. Lucarelli, C. Mazzocchi, M. L. Commara, L. Fortunato, A. Guglielmetti, F. Soramel, L. Stroe *et al.*, Study of the threshold anomaly effect in the reaction $^{7}Li + ^{208}Pb$ at energies around the Coulomb barrier, Eur. Phys. J. A **57**, 95 (2021).

[24] Y. Kucuk, V. Guimarães, and B. Carlson, Towards a systematic optical model potential for $a = 8$ projectiles, Euro. Phys. J. A **57**, 87 (2021).

[25] R. Akyuz and A. Winther, in Nuclear Structure and Heavy Ion Reactions, *Proceedings of Enrico Fermi International School of Physics*, edited by R. A. Broglia, C. H. Dasso, and R. Ricci (North-Holland, Amsterdam, 1979).

[26] D. T. Khoa and G. Satchler, Generalized folding model for elastic and inelastic nucleus-nucleus scattering using realistic density dependent nucleon-nucleon interaction, Nucl. Phys. A **668**, 3 (2000).

[27] D. T. Khoa, G. R. Satchler, and W. von Oertzen, Nuclear incompressibility and density dependent NN interactions in the folding model for nucleus-nucleus potentials, Phys. Rev. C **56**, 954 (1997).

[28] D. Pereira *et al.*, Nuclear rainbow in the $^{16}O + ^{27}Al$ system: The role of couplings at energies far above the barrier, Phys. Lett. B **710**, 426 (2012).

[29] L. M. Fonseca, R. Linares, V. A. B. Zagatto, F. Cappuzzello, D. Carbone, M. Cavallaro, C. Agodi, J. Lubian, and J. R. B. Oliveira, Elastic and inelastic scattering of ^{16}O on ^{27}Al and ^{28}Si at 240 MeV, Phys. Rev. C **100**, 014604 (2019).

[30] D. Pereira, C. Silva, J. Lubian, E. Rossi, L. Chamon, G. Nobre, and T. Correa, Understanding fusion suppression and enhancement in the $^{18}O + ^{58,60,64}Ni$ systems, Nucl. Phys. A **826**, 211 (2009).

[31] M. A. G. Alvarez, L. Chamon, M. Hussein, D. Pereira, L. Gasques, E. Rossi, and C. Silva, A parameter-free optical potential for the heavy-ion elastic scattering process, Nucl. Phys. A **723**, 93 (2003).

[32] A. Spatafora, F. Cappuzzello, D. Carbone, M. Cavallaro, J. A. Lay, L. Acosta, C. Agodi, D. Bonanno, D. Bongiovanni, I. Boztosun, G. A. Brischetto, S. Burrello, S. Calabrese, D. Calvo, E. R. Chávez Lomelí, I. Ciraldo, M. Colonna, F. Delaunay, N. Deshmukh, J. L. Ferreira *et al.* (for the NUMEN Collaboration), $^{20}Ne + ^{76}Ge$ elastic and inelastic scattering at 306 MeV, Phys. Rev. C **100**, 034620 (2019).

[33] D. Carbone, R. Linares, P. Amador-Valenzuela, S. Calabrese, F. Cappuzzello, M. Cavallaro, S. Firat, M. Fisichella, A. Spatafora, L. Acosta, C. Agodi, I. Boztosun, G. Brischetto, D. Calvo, E. Chávez Lomelí, I. Ciraldo, M. Cutuli, F. Delaunay, N. Deshmukh, P. Finocchiaro *et al.*, Initial state interaction for the $^{20}Ne + ^{130}Te$ and $^{18}O + ^{116}Sn$ systems at 15.3 AMeV from elastic and inelastic scattering measurements, Universe **7**, 58 (2021).

[34] I. Thompson, M. Nagarajan, J. Lilley, and M. Smithson, The threshold anomaly in $^{16}O + ^{208}Pb$ scattering, Nucl. Phys. A **505**, 84 (1989).

[35] D. Rifuggiato, L. Calabretta, and G. Cuttone, Cyclotrons and Their Applications, *Proceedings of the 17th International Conference Cyclotrons 2004*, Particle Acceleratory Society Japan (2004), p. 541.

[36] F. Cappuzzello, C. Agodi, D. Carbone, and M. Cavallaro, The MAGNEX spectrometer: Results and perspectives, Eur. Phys. J. A **52**, 167 (2016).

[37] D. Torresi, O. Sgouros, V. Soukeras, M. Cavallaro, F. Cappuzzello, D. Carbone, C. Agodi, G. Brischetto, S. Calabrese, I. Ciraldo, N. Deshmukh, A. Hacisalihoglu, L. L. Fauci, and A. Spatafora, An upgraded focal plane detector for

the MAGNEX spectrometer, Nucl. Instrum. Methods Phys. Res. A **989**, 164918 (2021).
[38] M. Cavallaro, F. Cappuzzello, D. Carbone, A. Cunsolo, A. Foti, A. Khouaja, M. R. D. Rodrigues, J. S. Winfield, and M. Bondì, The low-pressure focal plane detector of the MAGNEX spectrometer, Euro. Phys. J. A **48**, 59 (2012).
[39] D. Carbone, Signals of the giant pairing vibration in ^{14}C and ^{15}C nuclei populated by (^{18}O, ^{16}O) two-neutron transfer reactions, Euro. Phys. J. Plus **130**, 143 (2015).
[40] G. A. Brischetto, Data reduction of the ^{18}O + ^{48}Ti elastic and inelastic scattering at 275 MeV in the context of the NUMEN project, Il Nuovo Cimento C **45**, 96 (2022).
[41] F. Cappuzzello, M. Cavallaro, A. Cunsolo, A. Foti, D. Carbone, S. E. A. Orrigo, and M. R. D. Rodrigues, A particle identification technique for large acceptance spectrometers, Nucl. Instrum. Methods Phys. Res. A **621**, 419 (2010).
[42] F. Cappuzzello, D. Carbone, and M. Cavallaro, Measuring the ions momentum vector with a large acceptance magnetic spectrometer, Nucl. Instrum. Methods Phys. Res. A **638**, 74 (2011).
[43] M. Cavallaro, F. Cappuzzello, D. Carbone, A. Cunsolo, A. Foti, and R. Linares, Transport efficiency in large acceptance spectrometers, Nucl. Instrum. Methods Phys. Res. A **637**, 77 (2011).
[44] F. Cappuzzello *et al.*, Interplay of the elastic and inelastic channels in the ^{16}O + ^{27}Al scattering at E_{lab} = 280 MeV, Eur. Phys. J. A **52**, 169 (2016).
[45] NNDC, NUDAT 3.0 (2023), https://www.nndc.bnl.gov/nudat3/, accessed: March 2023.
[46] I. J. Thompson, Coupled reaction channels calculations in nuclear physics, Comput. Phys. Rep. **7**, 167 (1988).
[47] V. A. B. Zagatto, F. Cappuzzello, J. Lubian, M. Cavallaro, R. Linares, D. Carbone, C. Agodi, A. Foti, S. Tudisco *et al.*, Important role of projectile excitation in ^{16}O + ^{60}Ni and ^{16}O + ^{27}Al scattering at intermediate energies, Phys. Rev. C **97**, 054608 (2018).
[48] D. Carbone, J. L. Ferreira, S. Calabrese, F. Cappuzzello, M. Cavallaro, A. Hacisalihoglu, H. Lenske, J. Lubian, R. Magaña Vsevolodovna, E. Santopinto, C. Agodi, L. Acosta, D. Bonanno, T. Borello-Lewin, I. Boztosun, G. Brischetto, S. Burrello, D. Calvo, E. Chávez Lomelí, I. Ciraldo *et al.*, Analysis of two-nucleon transfer reactions in the ^{20}Ne + ^{116}Cd system at 306 MeV, Phys. Rev. C **102**, 044606 (2020).
[49] M. J. Ermamatov *et al.*, Comprehensive analysis of high-lying states in ^{18}O populated with (t,p) and (^{18}O, ^{16}O) reactions, Phys. Rev. C **96**, 044603 (2017).
[50] E. N. Cardozo, J. Lubian, R. Linares, F. Cappuzzello, D. Carbone, M. Cavallaro, J. L. Ferreira, A. Gargano, B. Paes, and G. Santagati, Competition between direct and sequential two-neutron transfers in the ^{18}O + ^{28}Si collision at 84 MeV, Phys. Rev. C **97**, 064611 (2018).
[51] E. Crema, D. R. Otomar, R. F. Simões, A. Barioni, D. S. Monteiro, L. K. Ono, J. M. B. Shorto, J. Lubian, and P. R. S. Gomes, Near-barrier quasielastic scattering as a sensitive tool to derive nuclear matter diffuseness, Phys. Rev. C **84**, 024601 (2011).
[52] E. Crema, V. A. B. Zagatto, J. M. B. Shorto, B. Paes, J. Lubian, R. F. Simões, D. S. Monteiro, J. F. P. Huiza, N. Added *et al.*, Reaction mechanisms of the ^{18}O + ^{63}Cu system at near-barrier energies, Phys. Rev. C **98**, 044614 (2018).
[53] J. L. Ferreira, D. Carbone, M. Cavallaro, N. N. Deshmukh, C. Agodi, G. A. Brischetto, S. Calabrese, F. Cappuzzello, E. N. Cardozo, I. Ciraldo, M. Cutuli, M. Fisichella, A. Foti, L. La Fauci, O. Sgouros, V. Soukeras, A. Spatafora, D. Torresi, and J. Lubian (NUMEN Collaboration), Analysis of two-proton transfer in the ^{40}Ca(^{18}O, ^{20}Ne) ^{38}Ar reaction at 270 MeV incident energy, Phys. Rev. C **103**, 054604 (2021).
[54] R. H. Bassel, G. R. Satchler, R. M. Drisko, and E. Rost, Analysis of the inelastic scattering of alpha particles. I, Phys. Rev. **128**, 2693 (1962).
[55] B. Pritychenko, M. Birch, B. Singh, and M. Horoi, Tables of E2 transition probabilities from the first 2^+ States in even-even nuclei, At. Data Nucl. Data Tables **107**, 1 (2016).
[56] T. Kibedi and R. H. Spear, Reduced electric-octupole transition probabilities, $B(E3; 0+ \quad 3-)$ - an update, At. Data Nucl. Data Tables **80**, 35 (2002).
[57] S. Raman, C. W. Nestor, and P. Tikkanen, Transition probability from the ground to the first-excited 2+ state of even-even nuclides, At. Data Nucl. Data Tables **78**, 1 (2001).
[58] N. Shimizu, T. Mizusaki, Y. Utsuno, and Y. Tsunoda, Thick-restart block Lanczos method for large-scale shell-model calculations, Comput. Phys. Commun. **244**, 372 (2019).